Stability of a Thin-Walled Silo Hopper – Case Study

Peter Knoedel

Dr Knoedel Engineering Consultants, Vordersteig 52, Ettlingen, D-76275, Germany
Professor of Steel Structures, Augsburg University of Applied Sciences, Germany

The paper presents a case study on an ensemble of four 60 m high, 8 m diameter concrete silos with steep steel hoppers of 10 mm / 8 mm wall thickness. A circumferential weld of one of the hoppers failed after some 6 months of operation.

The author was commissioned by the owner to give expert's opinion as to the reason of the failure. It seemed that non-axisymmetric loading ovalised the hopper and subsequently caused the weld to fail. However, the other hoppers showed deformation patterns in shape of longitudinal corrugations which were somewhat inclined against the cone meridians. So one of the options was that attaching outlet boxes after completing the hopper could have caused the deformations of the conical shells due to unsymmetric weld shrinkage – a type of failure, which is repeatedly encountered with thin walled above ground cylindrical tanks.

In order to identify the reasons of failure a numerical study was performed. First, unsymmetrical weld shrinkage was applied to cause distortions and residual stresses in the hopper. Second, unsymmetrical loading conditions due to funnel flow of the bulk solid were applied, and stability phenomena were investigated for this configuration. The paper presents results of the study and discusses different reasons for the failure of the circumferential weld.

1 Introduction

Several steel hoppers of a concrete four-in-a-row silo building for soy grist showed deformations after some 6 months of operation. 4 weeks later a circumferential weld failed in one of the hoppers at the transition of 10 mm to 8 mm by tearing along 1/4 of the circumference and some hundred tons of product poured out of the crack. Dr Knoedel Engineering Consultants were commissioned in 2008 by the owner to give expert's opinion on the cause of the failure.

In part poor welding was assigned to have contributed which seemed to be clear after the torn weld had been examined. However if poor welding was the exclusive reason of failure, the hopper should have been expected to fail shortly after filling the silo for the first time to the designed level. Besides, the structural analysis of the hopper showed, that even the poor weld should have withstood the design loads, if these were axisymmetric as assumed in the analysis.

It was clear that a non-axisymmetric situation was involved after rupture of the weld, therefore all deformations of the hopper which occurred after the failure of the weld should show features of non-axisymmetric loading.

Figure 1: Deformation of the hopper without subsequent failure (project anonymous) (photograph: P. Knoedel 2008)

Figure 2: Deformation of the outlet plate without subsequent failure (project anonymous) (photograph: P. Knoedel 2008)

However the deformations which were observed several weeks before failure and the type of failure itself supported the assumption, that ovalisation of the hopper occurred at first and subsequently caused local overloading of the hopper wall and triggered failure of the weld. On the above photographs (**Figure 1** and **2**) one of the silos is shown, that had typical deformations but did not fail.

The present paper reports on a numerical study in which different influences were investigated, which cause non-axisymmetric loading of the hopper-shell, such as unsymmetric flow of the bulk solid during discharge and residual stresses by weld

shrinkage, which were induced during assembly. The study was completed by the end of 2009. The data sets have been rerun recently for purpose of a consistent display in this paper.

2 Model

2.1 Geometry

An outline of the silo structure and the relevant dimensions are given in the following sketch (**Figure 3**).

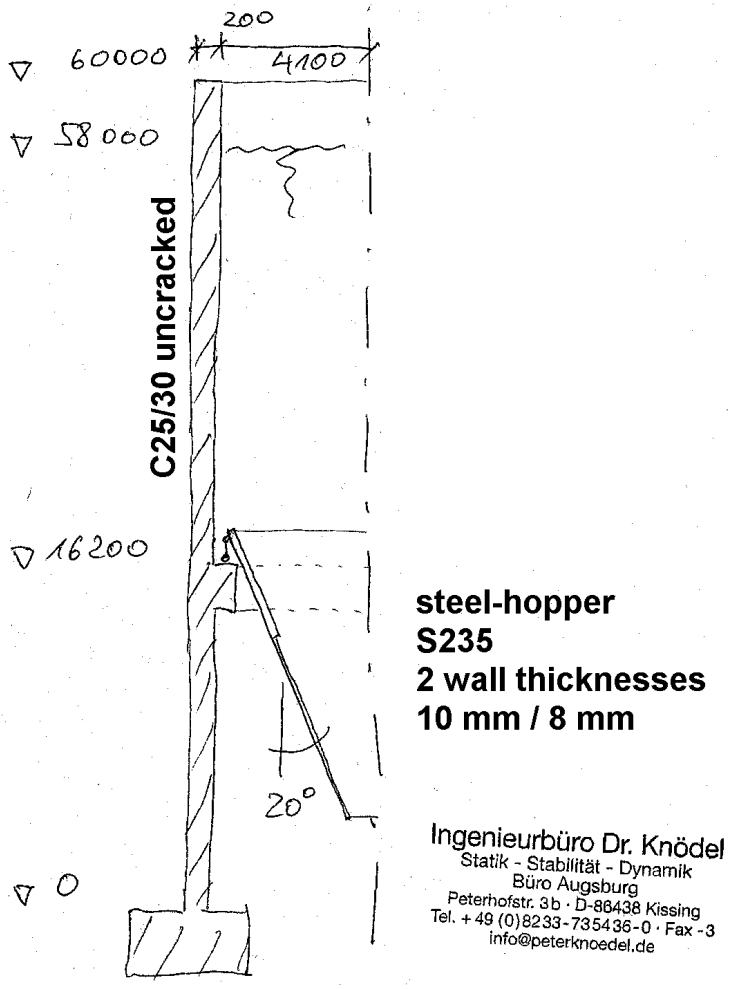

Figure 3: Elevation of the structure under consideration (not to scale)

The top edge of the hopper is integrated in an annular box girder of triangular shape, the inclined face of which is built by the conical shell of the hopper, the vertical face is built by a cylindrical plate 500x10 mm and the horizontal face, which is supported by a concrete ledge, is made up of an annular plate app. 200x30 mm.

The gap between the concrete silo wall and the vertical face of the annular girder is grouted, but there is no anchoring against lifting of the hopper's top edge.

The height of the hopper is app. 9800 mm, the 10 mm strake has a meridional length of 750 mm. At the bottom end there is a circular outlet of 1000 mm diameter with a square

outlet flange of 1200/1200 mm. (On the actual silo this might have been only 1100/1100 mm.)

A lateral outlet box 800 mm high and 500 mm wide is attached near the bottom end of the hopper, so that there is a clear vertical space of 500 mm between the bottom outlet plate and the bottom edge of the outlet box. This box was mounted when the hopper was still in place, so that the joining welds would induce an unsymmetric stress field to the hopper.

2.2 Support and Boundary Conditions

Due to the shape of the bulk solid's pressure distribution along the circumference a symmetry plane at 0° and 180° could be used.

Modeling the support with fixed nodes showed robust convergence up to the factorized design loads with some lifting forces along the top edge, but no local inclined folds at the outlet box as observed with the failed hopper.

When the model was improved by using contact elements LINK10, local lifting of the annular girder off the ledge and disconnecting from the concrete wall was satisfactory, but convergence grew very difficult even at nominal loads and local folds still could not be observed. Elastic restraint for the closed contacts was modeled such, that vertical and horizontal truss members of 500 mm length were inserted between the structure and the fixed supports. The axial stiffness of the truss members was equivalent to a continuous 10 mm steel plate.

For 'fixed supports' the truss members were switched to LINK8, so that a realistic flexibility of the supports was given in that case as well.

2.3 Gridsize and Meshing

The structure was meshed with ANSYS SHELL181 with full integration option.

The classical chessboard pattern buckle of a cylinder under axial compression has a half-wave length of
$L,crit = 3{,}46 \sqrt{(R*T)} = L,bend * \sqrt{2}$
(see e.g. Knoedel 2008 [1]), the axisymmetrical bending half-wave length amounts to
$L,bend = 2{,}44 \sqrt{(R*T)}$.

For cones we substitute R by the radius of curvature
$R,curv = R / \cos \beta$,
with β being the inclination of the meridian against the vertical.

For the present cone we receive
$R,max,curv = 4000 \text{ mm} / \cos 20° = 4257 \text{ mm}$
$R,min,curv = 500 \text{ mm} / \cos 20° = 532 \text{ mm}$
and thus having bending half-waves of
$L,bend,max = 2{,}44 \sqrt{(4257 \text{ mm} * 8 \text{ mm})} = 450 \text{ mm}$
$L,bend,min = 2{,}44 \sqrt{(532 \text{ mm} * 8 \text{ mm})} = 159 \text{ mm}$

With 4-node-Elements we should have at least 5 elements per half-wave (Knoedel 2003 [2]), giving maximum element sizes in meridional direction of 90 mm at the top

and 32 mm at the bottom of the cone. As far as elastic buckling is concerned, the element size in circumferential direction should not exceed 90 mm * √2 = 127 mm at the top and 32 mm * √2 = 45 mm at the bottom.

The actual element size was controlled by a parameter EFAK which was used as divisor for a basic element size of 1000 mm. Studying convergence of the results for different values of EFAK (2 to 24) showed that membrane stresses were stable at EFAK = 8, but radial displacements of the shell required EFAK = 16. The element sizes in the cone resulted to be 218 mm (circumferential) and 53 mm (meridional) at the top and 28 mm (circumferential) and 56 mm (meridional) at the bottom. We would not want to use an even smaller element size because of the duration of the nonlinear runs. It is obvious, that the shell is given to much bending stiffness artificially in out of plane bending, which in return makes the results lower bounds of out-of-plane displacements and of buckling loads.

2.4 Material

According to the manufacturer steel plates S235 were used. The properties were taken to be 210.000 N/mm^2 for Young's modulus and 0,3 for Poisson's ratio. Yield limit was set to 240/1,1 N/mm^2. After yielding isotropic hardening was used, the slope in the plastic range was taken to be

(360 N/mm^2 – 240 N/mm^2) / 0,2 = 600 N/mm^2

which describes a sloped transition from yield to tensile stress along 20 percent of plastic strain.

2.5 Bulk Solid

The silo under consideration is used to handle coarsely ground soy beans (soya grist). Material parameters were determined from samples which were taken after the hopper failed. The material parameters used in calculation are given in table 1:

Table 1: Properties of the soy grist

Characteristical values derived from testing	**Remark**
6,9 – 8,4	γ [kN/m3] unit weight
31 – 41	φ [°] angle of internal friction
0,40 – 0,49	λ [–] stress ratio horizontal/vertical
0,37 – 0,60	μ [–] coefficient of wall friction – hopper (steel – smooth wall)
0,34 – 0,56	μ [–] coefficient of wall friction – bin (slipformed concrete – smooth wall)

Remark:
The given upper and lower limits are not actually test results; the coefficients of variation given in DIN 1055-6:2005 table C.2 [3] are fitted to mean and scatter received from the tests.

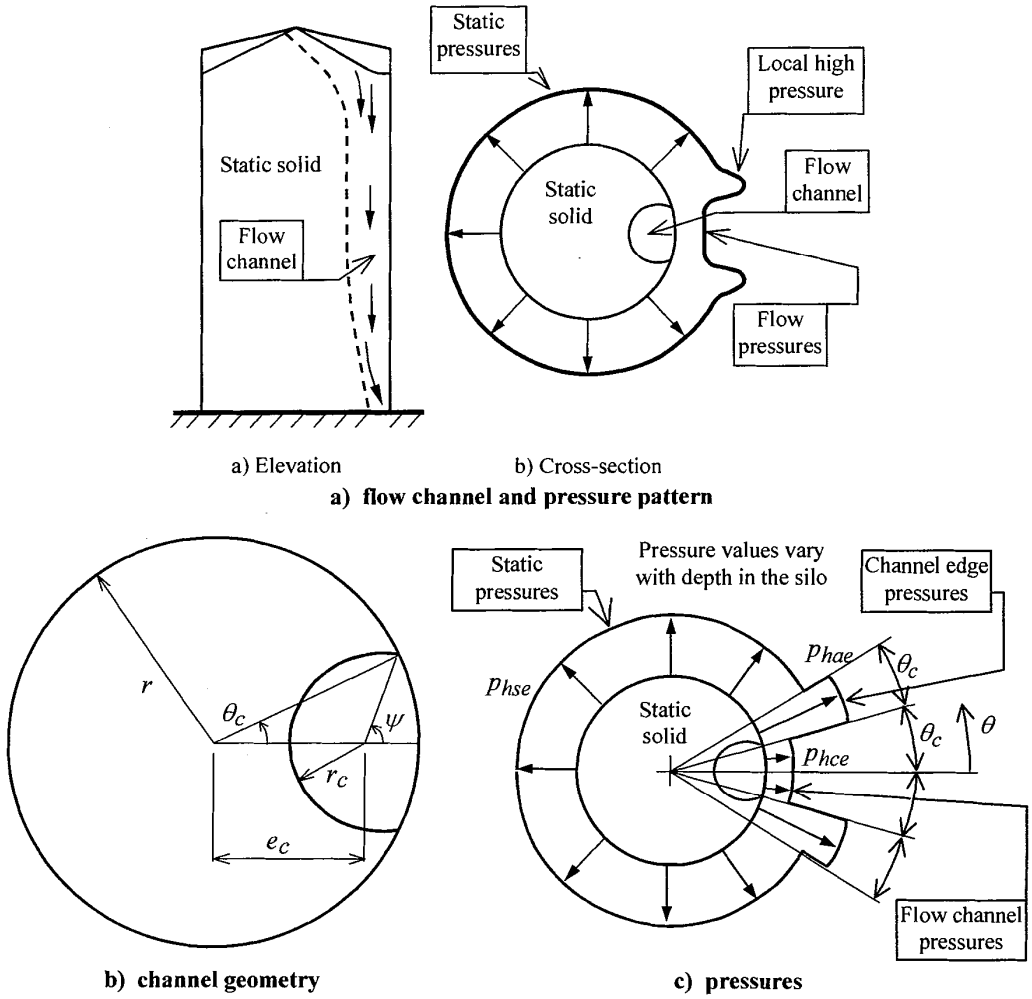

Figure 5.5: Eccentric discharge flow channel and pressure distribution

Figure 4: Geometry and circumferential pressure distribution with funnel flow according to EC1-4 fig. 5.5 [4] (DIN 1055-6 fig. 13 [3] is identical)

Funnel flow along the hopper's wall was simulated by using the circumferential pressure distribution given in DIN 1055-6:2005 [3] for cylindrical slender silo bins (see **Figure 4**). It should be noted, that there are no provisions for funnel flow in the hopper itself. For simplicity, the circumferential angle Θ,c of the flow channel was kept constant within the hopper, so that the actual width is decreasing from top to bottom. This might be not quite coincident with the state of flow within the bottom of the hopper, but it is by far on the safe side, since this approach does exert much smaller unsymmetrical loads to the hopper's wall.

The variation of the pressures along the hopper's height was modeled according to the provisions of DIN 1055-6 [3].

Remark: The regulations coincide with those of EC1-4 [4].

2.6 Weld Shrinkage

'Weld Shrinkage' – which is in common used synonymously for the shrinkage of the HAZ (heat affected zone) until reaching ambient temperature again – was modeled by applying an effective shrinkage potential (Mang/Knödel 1982 [5]) rather than modeling temperature fields as well as material's phase changes and their subsequent field of residual stresses. It seems that this will do to show the effect and besides it has the advantage, that a standard commercial FEA package can be used. Experience shows that you should apply plastic strain within the HAZ (Loose 2009 [6]).

$\varepsilon,pl = -240\ N/mm^2 / 2{,}1*10^5 = -1{,}14*10^{-3} = -0{,}11\ \%$

This corresponds to a substitute temperature drop of

$\Delta T = -1{,}14*10^{-3} / (1{,}2*10^{-5} * 1/K) = -95\ K$

Due to the material law which has a comparatively small stiffness after exceeding the yield limit it does not matter significantly, whether you apply this strain or a more realistic strain history for temperatures under 800°K because of the development of the yield limit along with elevated temperatures.

In the present study a temperature difference of –100°K was used for elements within a distance of 40–45 mm from the weld, which seems to be a sound engineering approach. After interpretation of first results a temperature difference of –300°K was chosen to be applied.

2.7 Geometrical Imperfections

For simplicity we decided not to use geometrical substitute imperfections.

On one hand, it is difficult which level of imperfections you need for engineering purposes (Knoedel / Ummenhofer / Schulz 1995 [7]). On the other hand, if your structure is very much affected by out-of-plane bending (which presently is the case) rather than having an evenly loaded membrane state, you can interpret this loads as 'load imperfections' and geometrical imperfections can possibly be avoided (Knoedel / Ummenhofer 2004 [8]).

3 Procedure

In a first step shrinkage in terms of differential temperature was applied to the model, stresses and deformations were calculated. In a second step additional filling loads from bulk solid were applied. Arbitrarily those were increased up to more than double the nominal loads.

A Newton-Raphson procedure was used for nonlinear path tracing employing both, geometrical and material nonlinearity. The former is needed to tackle the shape deformations of the thin-walled conical shell with the possibility of passing beyond bifurcation points (Knoedel/Ummenhofer 2004 [8]). The latter is needed to allow for yielding of the HAZ, e.g. at hot-spot corners of the outlet box.

The factorized load configuration was approached e.g. by 10 % steps of the nominal load, allowing for bisection in case of convergence problems near a limit point or at a step change of stiffness, if contacts alter their status.

Accompanying linear eigenvalue analyses were performed at intermediate load increments in order to identify possible mode-changes along the prebuckling path. In a first step no contacts were used for this feature.

4 Results

If not stated otherwise results are given for contact support conditions.

Symbols in load-displacement-diagrams mark a selection of results; there might be more in between, which are not shown for technical reasons.

4.1 Weld Shrinkage

Due to the different stiffness properties in the meridional and circumferential direction the maximum stress response of the structure to the above shrinkage strain of –100°K is

168 N/mm^2 in meridional direction
116 N/mm^2 in circumferential direction
as well as
app. 0,0003 equivalent plastic membrane strain at the top edge of the outlet box. The given stresses are located at the longitudinal or lateral edge of the cutout of the outlet box. Aside of these pretensioned strips patches of compressive stresses developed, having maxima of about 50-60 Nmm^2.

Alternatively the threefold shrinkage has been applied, i.e. a temperature drop of –300°K which produced
195 N/mm^2 in meridional direction
213 N/mm^2 in circumferential direction
as well as
app. 0,004 equiv. plastic membrane strain – vertical edge of the outlet box
app. 0,002 equiv. plastic membrane strain – top horizontal edge of the outlet box
(see **Figures 5-7**). Aside of the vertical edge a compressive strip with 40-80 N/mm^2 developed.

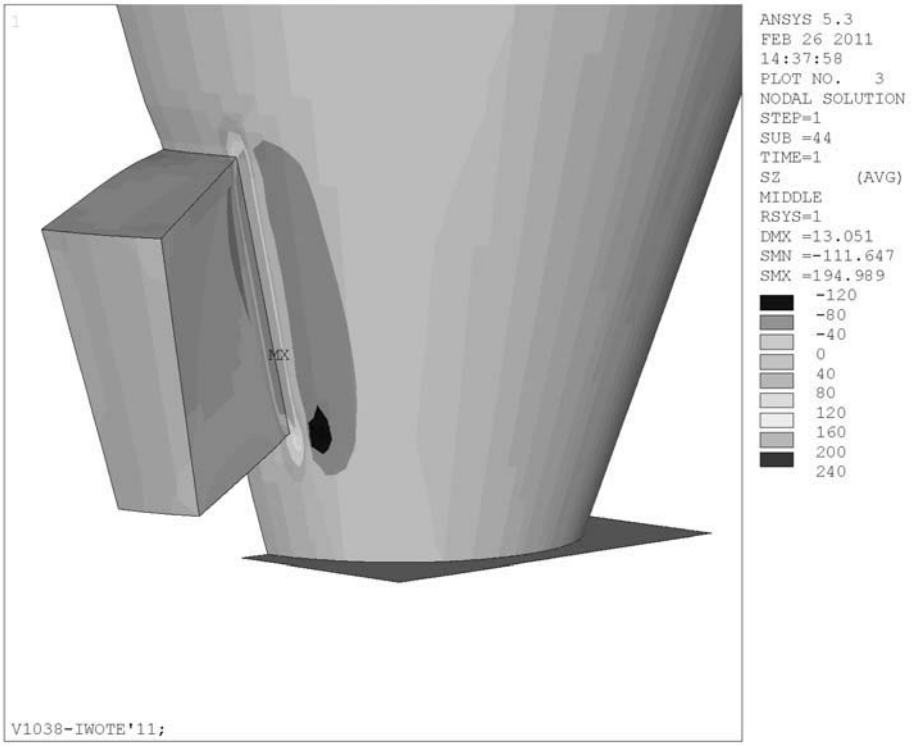

Figure 5: Meridional membrane stresses at the outlet box (–300°K)

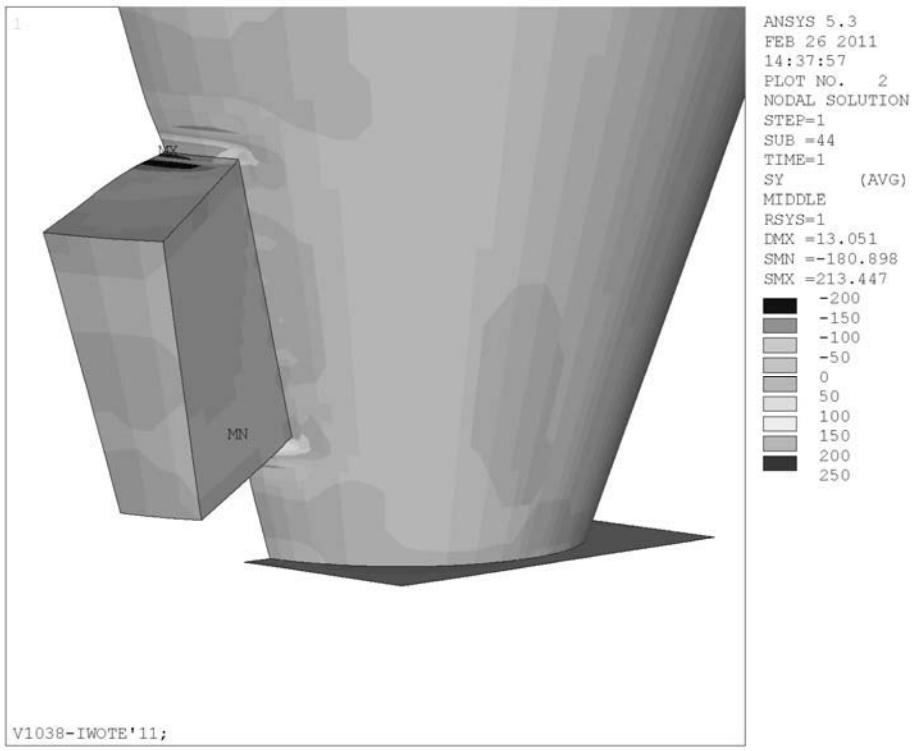

Figure 6: Circumferential membrane stresses at the outlet box (–300°K)

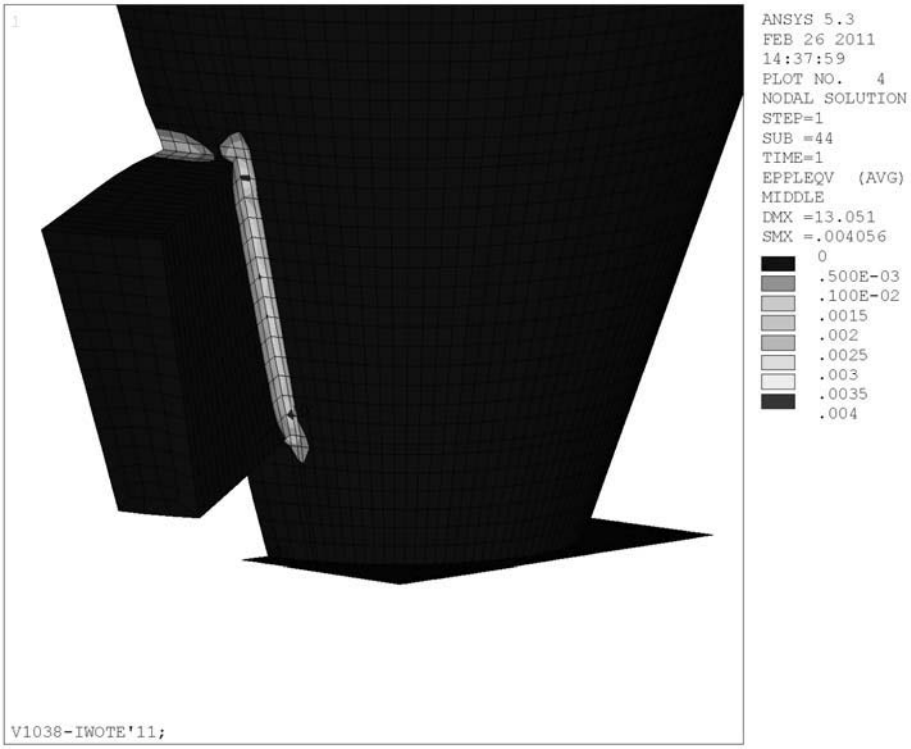

Figure 7: Plastic membrane equivalent strain at the outlet box (–300°K)

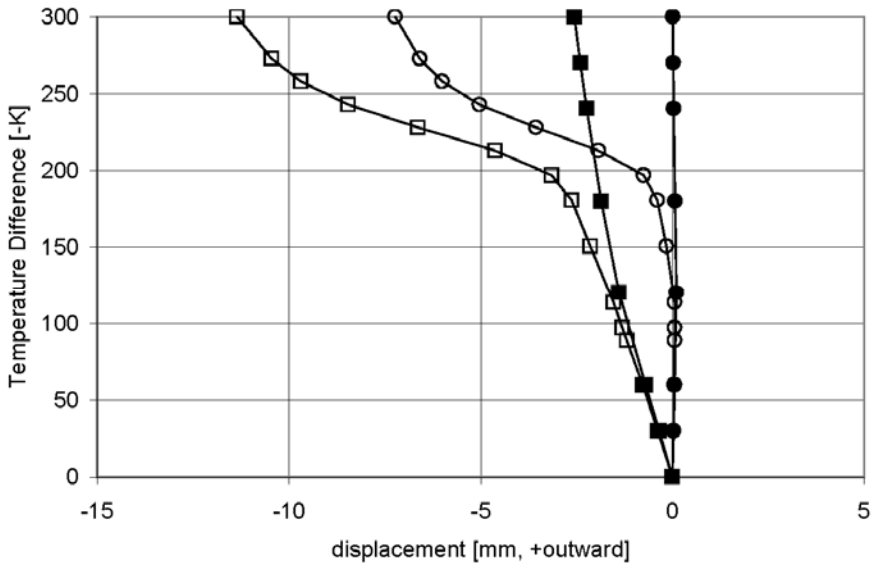

square symbols: top corner; circular symbols: neighbor 19° aside
filled symbols: fixed supports; hollow symbols: contact supports

Figure 8: Radial nodal displacements at the outlet box

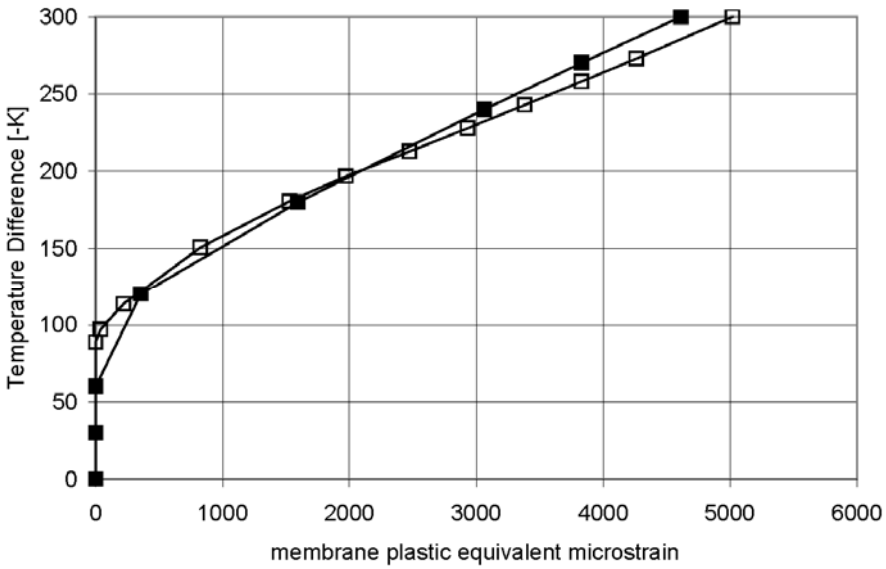

filled symbols: fixed supports; hollow symbols: contact supports

Figure 9: Development of plastic membrane equivalent strain at the outlet box

4.2 Bulk Solid

For verification axisymmetric loads from bulk solid – normal surface pressure and wall friction – were applied. The stresses coincided with manual calculations.

4.3 Interaction of Weld Shrinkage and Bulk Solid

The results of the model, loaded by –300°K temperature difference along the welding seams of the outlet box and subsequently loaded by 200 % of the nominal filling load are shown in the following **Figures 10-19**.

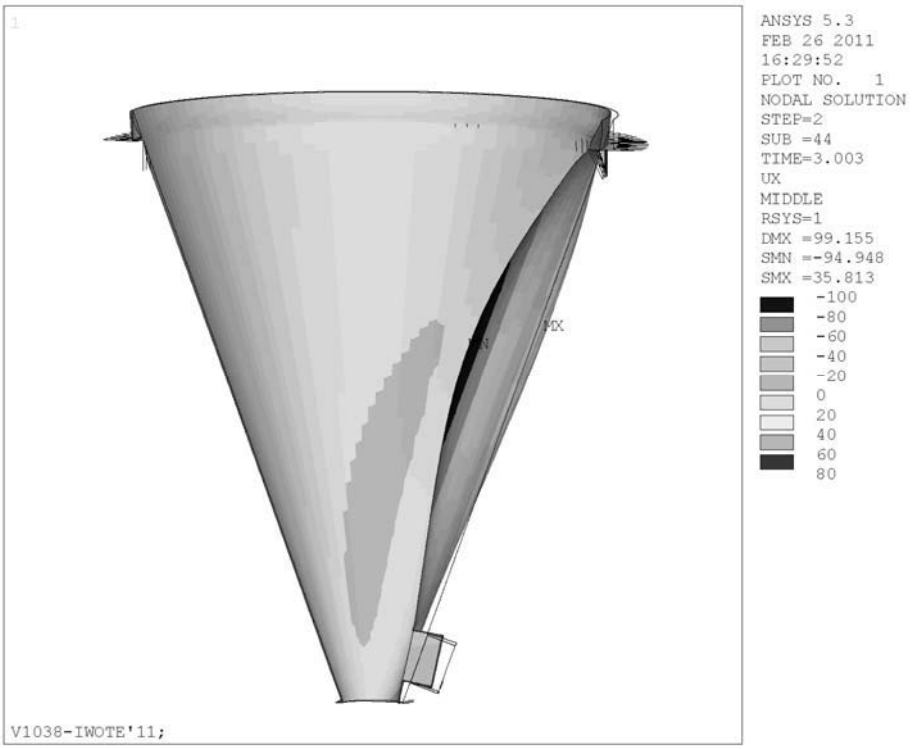

Figure 10: Radial deformations at 200 % filling load

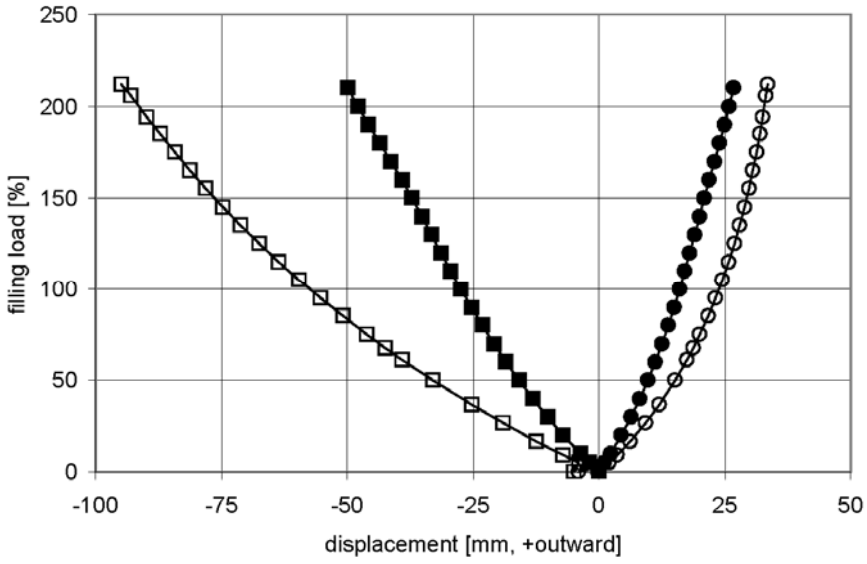

square symbols: luff meridian; circular symbols: neighbor 38° aside
filled symbols: fixed supports; hollow symbols: contact supports

Figure 11: Radial nodal displacements at mid-height of the luff meridian

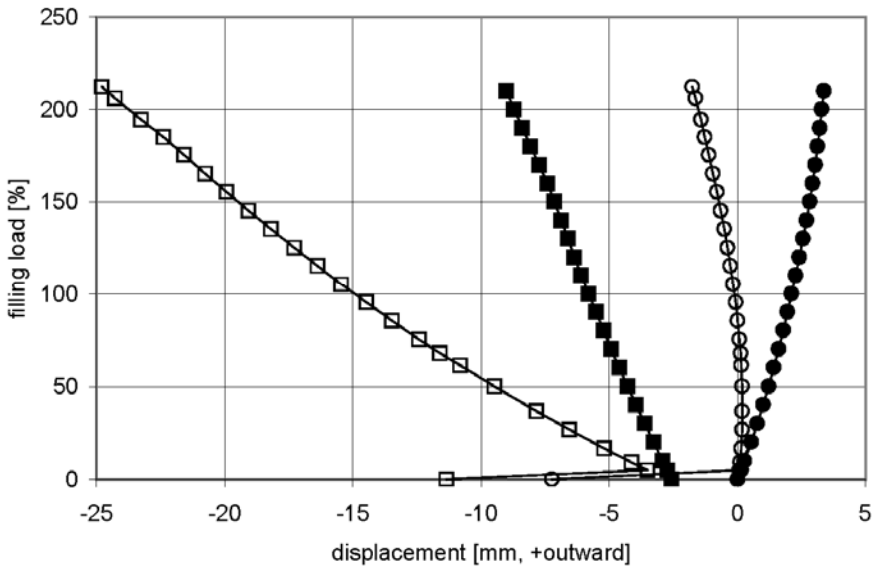

square symbols: top corner; circular symbols: neighbor 19° aside
filled symbols: fixed supports; hollow symbols: contact supports

Figure 12: Radial nodal displacements at the outlet box

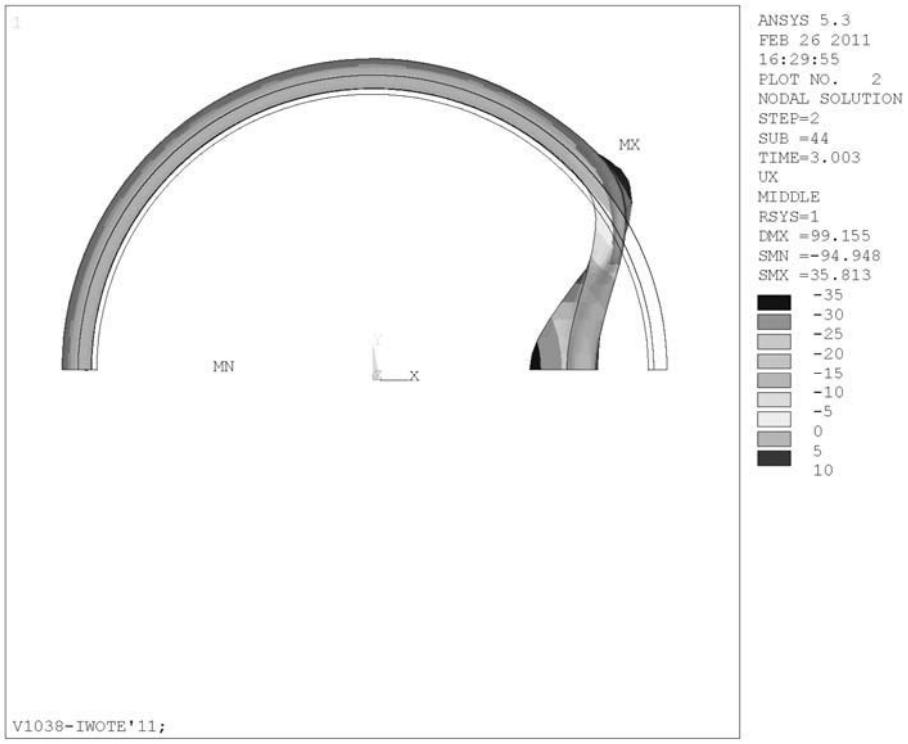

Figure 13: Radial deformations of the top supporting ring at 200 % filling load

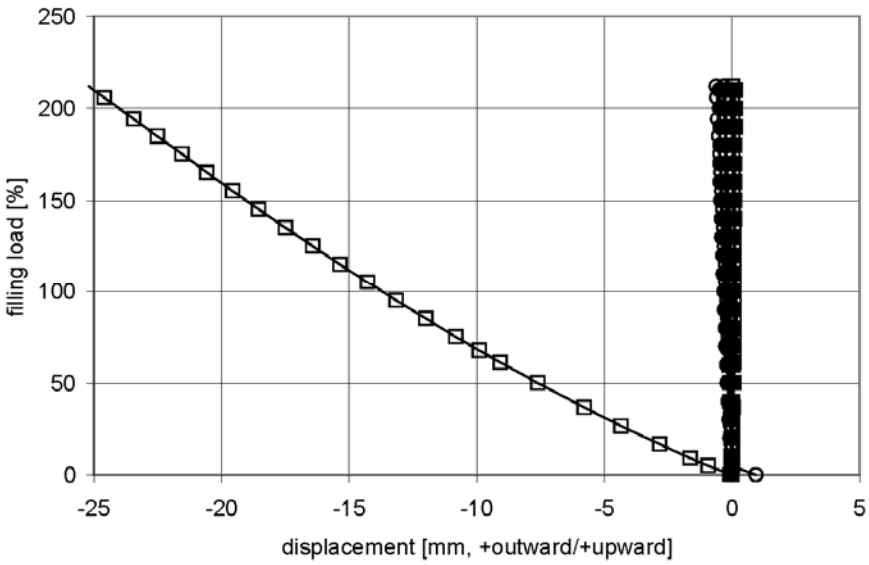

square symbols: luff; circular symbols: neighbor 38° aside
filled symbols: fixed supports; hollow symbols: contact supports

Figure 14: Radial and vertical displacements of selected nodes of the top supporting ring

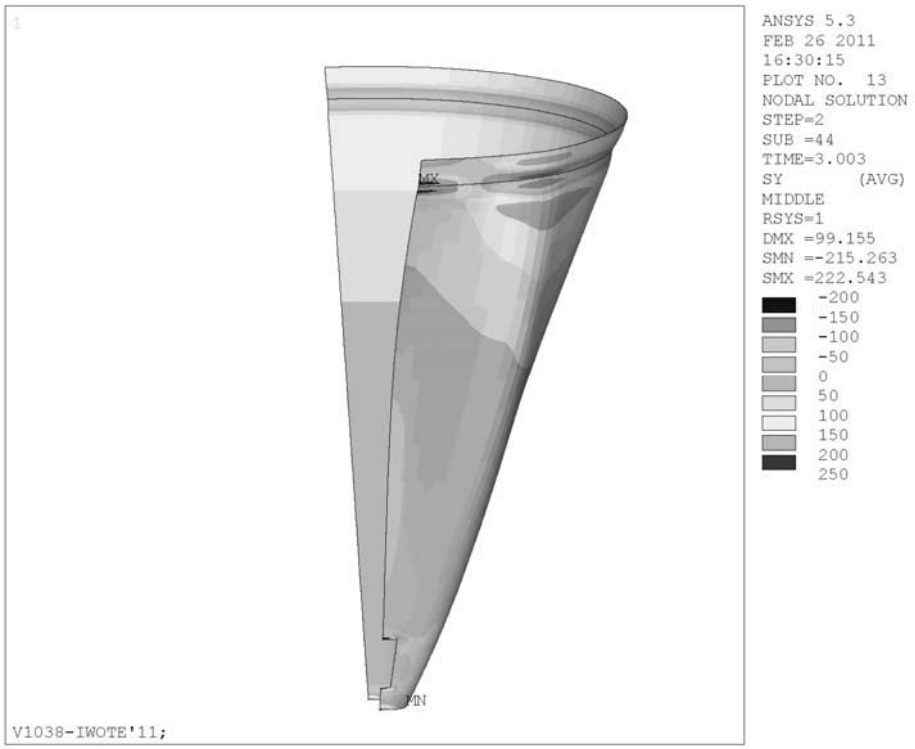

Figure 15: Circumferential membrane stresses at 200 % filling load

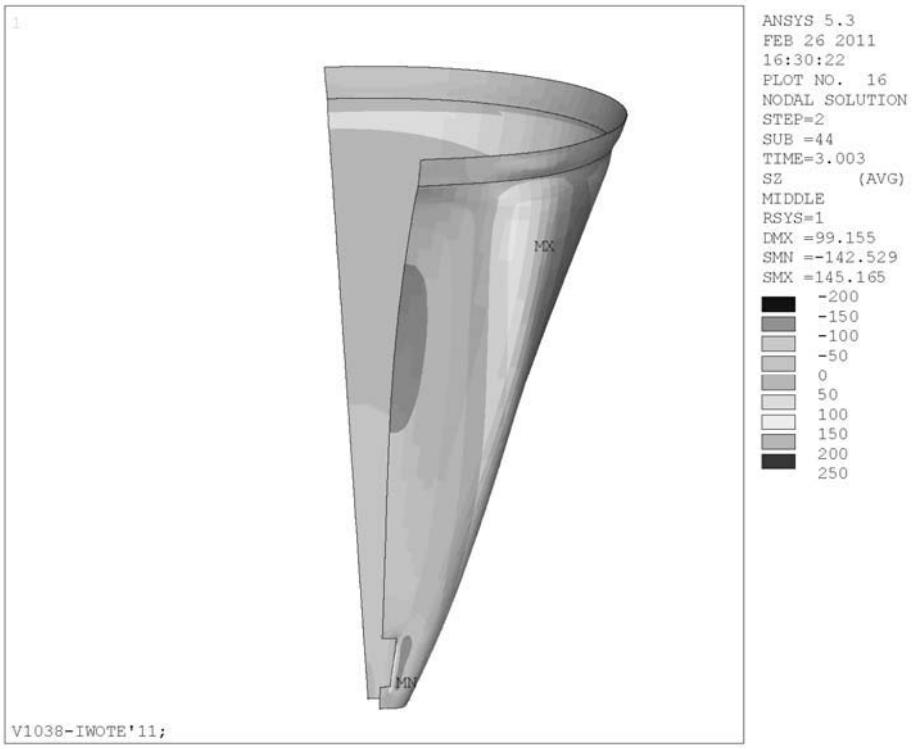

Figure 16: Meridional membrane stresses at 200 % filling load

Figure 17: Plastic equivalent membrane strain at 200 % filling load

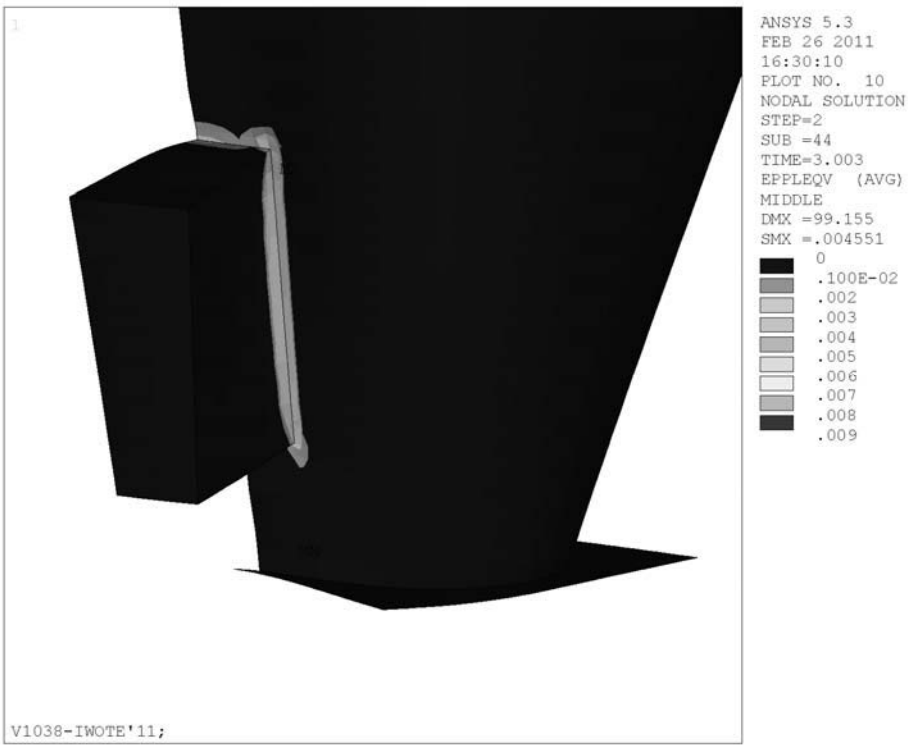

Figure 18: Plastic equivalent membrane strain at 200 % filling load

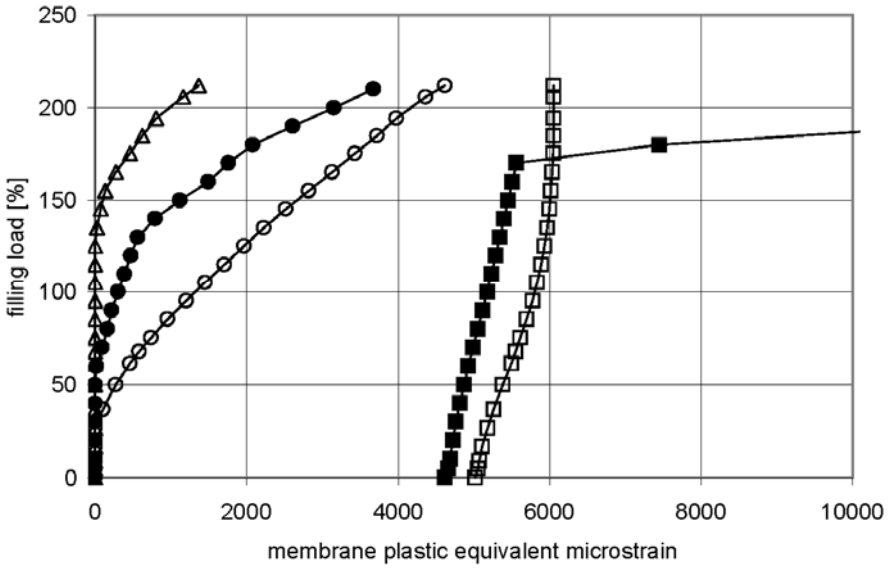

square symbols: top corner of the box;
circular symbols: upper part of hopper
triangular symbols: bottom outlet flange
filled symbols: fixed supports; hollow symbols: contact supports

Figure 19: Plastic equivalent membrane strain at selected nodes

4.4 Stability

The following plots (**Figures 20-21**) show shell eigenmodes of selected load steps, each associated with the lowest load factors. There were lower critical loads, but these belonged to deformation modes of the outlet box.

For comparison, data of a calculation by hand according to DIN 18800-4 [9] is given for the top edge of the 8-mm-strake and a hoop stress of 78 N/mm^2, which occurs at 100 % of axisymmetrical filling load:

critical meridional stress 251 N/mm^2, characteristical meridional buckling resistance 121 N/mm^2;
critical circumferential stress 13,2 N/mm^2, characteristical circumferential buckling resistance 8,6 N/mm^2;

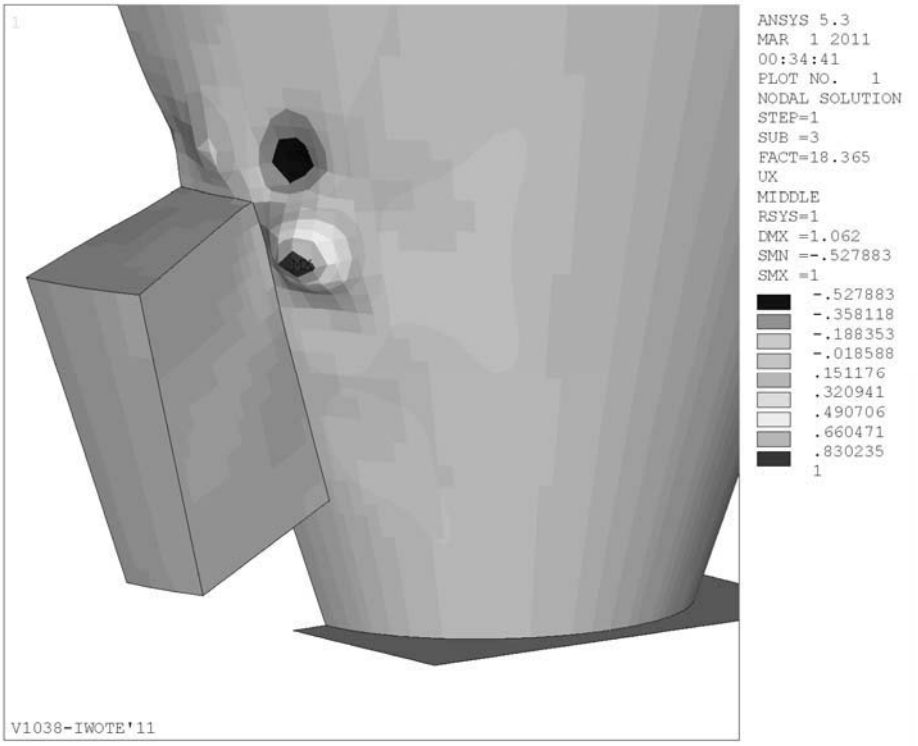

Figure 20: Mode for lowest critical load factor 18,4 associated with deformations adjacent to the outlet box at 10 % nominal filling load

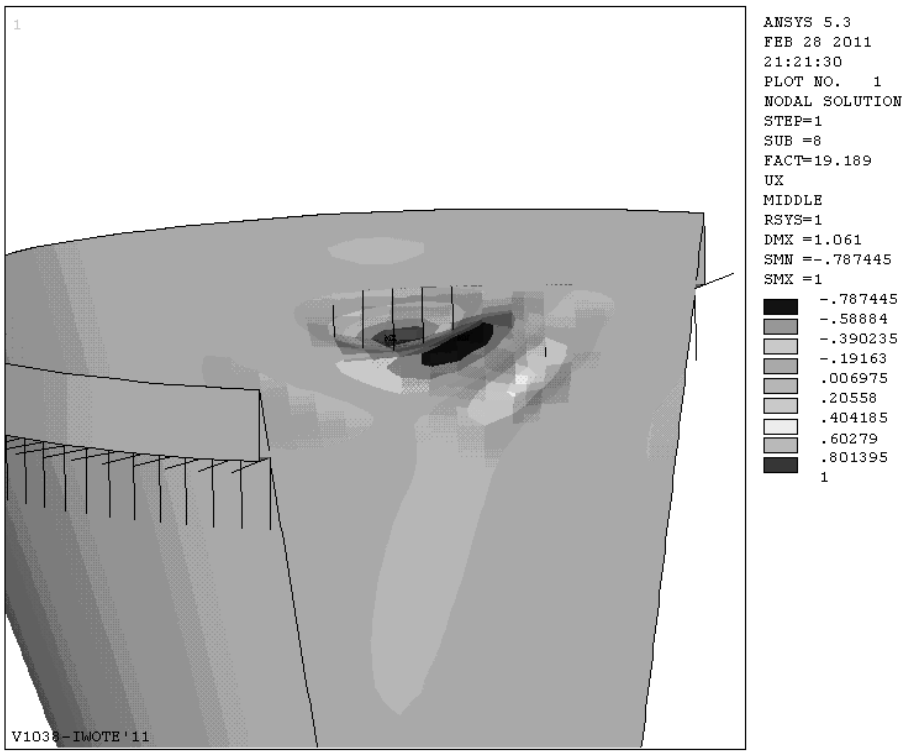

Figure 21: Mode for lowest critical load factor 19,2 associated with shell deformations at 20 % nominal filling load

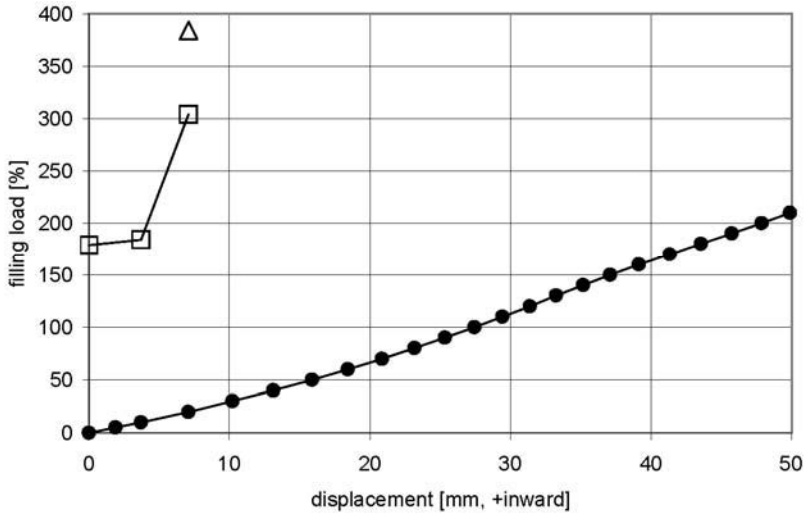

circular symbols: mode shapes with deformations at luff meridian (none)
triangular symbols: mode shapes with deformations at upper cone
square symbols: mode shapes with deformations at outlet box

Figure 22: Accompanying linear eigenvalues vs. displacement of luff meridian at mid-height

5 Conclusions

The above results give rise to the following conclusions:

– At such a flexible structure applying a temperature difference of –100°K corresponding to a shrinkage of 1,2 per mille might not be sufficient to introduce welding residual stresses at the yield limit.
Apropriate results were obtained by applying –300°K corresponding to a shrinkage of 3,6 per mille (see **Figure 9**).

– In the case of contact supports the radial nodal displacements at the outlet box show a feature which is associated to a global strainless mode of the weightless hopper: opposite to the outlet box the supporting ring is lifting of it's supports so that the complete structure is tilting and the bottom part of the hopper is moving leeward (see **Figure 8**).
After applying filling load this feature is reversed during the first load substep (see **Figure 12**).
In both cases, fixed or contact supports, the plastic equivalent membrane strain at the outlet box has the same intensity (see **Figure 9**).

– The welding residual stresses at the outlet box cause considerable local inward deformations of the box, as should have been expected (e.g. Loose 2008 [10], [11], Banke / Schmied / Schulz 2003 [12]). However, they don't seem to cause critical warping of the cone, as was expected with respect to typical failures with cylindrical tanks (Knödel / Wolfmüller 1990 [13], Mang / Knödel 1994 [14]).

– The assumed funnel flow along 19° of each side of the luff meridian causes considerable out of plane deformations to the inside of the hopper (as could have been expected – reduction of the wall pressure by the funnel is equivalent to a load, which would give wall pressure from the outside).
Equilibrium along the circumference is sustained by a supporting arch, which develops in the bulk solid around the funnel and is footed at both sides of the funnel at the hopper wall, giving a patch of high pressure to the outside (see **Figure 4**).

– These two effects cause the bottom outlet plate to warp (see **Figure 18**), but plastic deformations in the bottom plate do not happen before 150 % of the nominal filling load (see **Figure 19**). Since plastic in-plane deformations were observed at the outlet plate, one might conclude, that the flow conditions inside the hopper, i.e. size and pressure distribution of funnel and supporting arch, were significantly worse than assumed in the above calculations.

– The above described unsymmetric loading condition causes the supporting ring to undergo a local displacement to the inside of the hopper (see **Figure 13** – rather we did expect a global cos-2-φ ovalisation).
Classical strainless mode deformation suggests, that this gross out of roundness deformation should coincide with warping of the edges of the shell, i.e. lifting off the support in certain parts of the supported circumference. However this effect could not be observed (see **Figure 14**); we assume that

possible lifting is counterweighted by the bulk solid's weight and wall frictional drag.

– There are only moderate circumferential membrane stresses at the bottom of the hopper, as is known (see **Figures 15** and **16**). These do not cause additional plastic deformations at the outlet box, so that the bottom area of the hopper would fail by rupture.
The critical part seems to be the top edge of the cone, where progressive membrane yielding is indicated (see **Figure 17**). The bending stresses at both surfaces of the shell as well as plastic surface bending strains (not documented in this paper for space restrictions) are by a factor of 2 higher at least. Usually in thin-walled shell design bending stresses are not a big issue, since overloading yields off bending stresses and after performing the necessary large radial deformations the shell structure arrives at a new and robust membrane state.
In the present case, were a faulty weld at the top supporting ring is in discussion, the described stress-and-strain state could very well explain the failure of the weld.

- Since the patch of circumferential compressive stresses around the luff meridian is only very small (see **Figure 15**), we would not expect buckling 'under external pressure' to occur for this load configuration.

- We have a patch of meridional compressive stresses around the luff meridian in excess of 100 N/mm^2, wide enough to trigger buckling under axial compression. According to the results of a classical buckling calculation, which were given in section 4.4, we would expect a linear eigenvalue (i.e. calculated at very low prestressing loads) to occur at 250 % of the nominal filling load. The mode shown in **Figure 20**, associated with app. 180 % filling load could be interpreted as being roughly around that order of magnitude, but the mode shape indicates, that this mode could rather have been triggered by the compressive stresses around the outlet box, which were caused by the weld shrinkage.

- We expect accompanying eigenvalues to decrease with increasing prebuckling deformation (**Figure 22**). It is known however from cylinders under internal pressure, that accompanying eigenvalues rise with increasing prebuckling deformation, but at a smaller slope, so they would intersect the prebuckling path near the limit point (Knödel 2005 [15]). With the present structure considerable numerical difficulties occured for prebuckling loads above 25 %. The Sturm sequence procedure seemed to fail or produced converged eigenvalues around $\lambda = 50$, which can be falsified for this hopper with large-area meridional compressive stresses above 100 N/mm^2 (see **Figure 16**). The reason might be a faulty geometry, originated by use of bi-linear elements along warping areas (Evert / Schweizerhof 2005 [16]). Additional effort is needed at this problem.

- As stated above, geometrical imperfections were not used in the above study, because the radial deformations of the hopper due to the variation of the wall pressure around the funnel could possibly be sufficient to bring the structure into a prebuckling state with adequate out of plane bending of the shell.

However this could have been a premature assumption because Sadowski and Rotter (2010 [17] and 2011 [18]) use axisymmetric weld depressions and non-axisymmetric radial initial imperfections additional to the funnel flow pressure pattern along the silo wall.

- The inclined fold at the top corner of the outlet box (see **Figure 1**) could not be obtained as a result of the calculations. Maybe modeling the outlet box with vertical faces along a meridian instead of parallel turns out to be an unsuitable simplification. This seems to require more thorough investigations.

6 Summary

The present paper reports on a study on a hopper of a soy grist silo, which has failed during operation.

A FEA study should verify the suspected reasons of the failure, which were a faulty circumferential weld and ovalisation due to funnel flow and/or a non-axisymmetric assembled outlet box at the side of the hopper.

The numerical results are presented and discussed in detail. Hints for future work are given.

7 Acknowledgements

Hard- and software for the presented FEA calculations have been sponsored by ANAKON GmbH, Karlsruhe (see www.anakon.de). Their support is gratefully acknowledged.

8 References

[1] Knoedel, P.: Recent Silo Codes – and still Structural Failure? pp 113-122 in: Chen, J.F., Ooi, J.Y., Teng, J.G. (eds): Structures and Granular Solids – From Scientific Principles to Engineering Applications. An international conference in celebration of the 60th birthday of Prof. J. Michael Rotter, The Royal Society of Edinburgh, Scotland, UK, 1-2 July 2008. Taylor & Francis Group, London 2008. (invited lecture)

[2] Knoedel, P.: Lecture notes on silos and tanks (in German). University of Applied Sciences, Karlsruhe, 2003. Updated regularly until 2007. Download from www.peterknoedel.de/lehre/V0309_FH-KA/behaelter.htm

[3] DIN 1055 Part 6: Design loads for buildings and loads in silo bins. March 2005. Amendment 2006.

[4] DIN EN 1991 (EC1): Eurocode 1: Actions on structures. Part 4: Silos and tanks; German version EN 1991-4:2006. 2006.

[5] Mang, F., Knödel, P.: Schweißen und Schweißverbindungen. Abschnitt 9.3 in: Stahlbau Handbuch – Für Studium und Praxis. 2. Auflage, Band 1, Stahlbau-Verlags-GmbH, Köln 1982. S. 427-444. (Welding and welding joints in steel structures handbook)

[6] Loose, T.: Private communication, 14.10.2009.

[7] Knoedel, P., Ummenhofer, T., Schulz, U.: On the Modeling of Different Types of Imperfections in Silo Shells. EUROMECH Colloquium 317, University of Liverpool, 21.-23. March 1994. Thin-Walled Structures 23 (1995), pp. 283-293.

[8] Knoedel, P., Ummenhofer, Th.: Design of Squat Steel Tanks with R/T > 5000. TP056 in Motro, R. (ed.): Proc., IASS Symposium: Shell and Spatial Structures from Models to Realization, Montpellier, 20-24 September 2004.

[9] DIN 18800: Steel structures. Part 4:2008-11 Stability – Analysis of safety against buckling of shells.

[10] Loose, T.: Einfluss des transienten Schweißvorganges auf Verzug, Eigenspannungen und Stabilitätsverhalten axial gedrückter Kreiszylinderschalen. Dissertation Karlsruhe 2008. (Influence of the transient welding process on distortion, residual stresses and stability of axially compressed cylindrical shells. PhD Karlsruhe 2008.)

[11] Loose, T., Ilieva, R.: Distortion of Circumferential Welds of Cylindrical Shells with Respect to Tacking and Welding Sequence. P. 181-190 in Vollertsen, F., Sakkiettibutra, J. (eds): Thermal Forming and Welding Distortion. Proceedings of the IWOTE'08: Int. Workshop on Thermal Forming and Welding Distortion, Bremer Institut für angewandte Strahltechnik, April 22-23, 2008.

[12] Banke, F., Schmied, J., Schulz, U.: Der Einfluss von Schweißeigenspannungen und Schweißverformungen auf das Beulverhalten von axialgedrückten Zylinderschalen. Stahlbau 72 (2003), Heft 2, S. 91-101. (Influence of welding residual stresses and welding distortions on the buckling behaviour of axially compressed cylindrical shells)

[13] Knödel, P., Wolfmüller, F.: Geometric Deviations and Structural Behaviour of Tanks and Silos. Colloquium "Requirements to the Tank-Structures Geometrical Shape", IASS Working Group I "Pipes and Tanks", Sept. 18-20, 1990, Varna, Bulgaria.

[14] Mang, F., Knoedel, P.: Repair of Tank-Structures, pp 255-257 in: Rao, V.J., Rao, P.D.P., Goli, H.B. (eds.): Rehabilitation, Renovation and Repairs of Structures, Tata McGraw-Hill Publishing Company Ltd., New Delhi 1994.

[15] Knödel, P.: Stabilitätsuntersuchungen an kreiszylindrischen stählernen Siloschüssen. Dissertation, Universität Karlsruhe 1995. (On the stability of circular cylindrical steel silo strakes.)

[16] Ewert, E., Schweizerhof, K.: On artificial geometry errors in the adaptive analysis of eigenvalues and eigenmodes of curved shell structures using the finite element method. Proc. Appl. Math. Mech. 5, 231-232 (2005).

[17] Sadowski, A.J., Rotter, J.M.: Study of Buckling in Steel Silos under Eccentric Discharge Flows of Stored Solids. J. Eng. Mech. 136 (2010), pp. 769-776.

[18] Sadowski, A.J., Rotter, J.M.: Buckling of very slender metal silos under eccentric discharge. Eng. Struct. 33 (2011), pp. 1187-1194.